JOURNAL OF SOLID STATE CHEMISTRY 43, 204–212 (1982)

Magnetic Behavior in the System $La_xGd_{1-x}TiO_3$

J. P. GORAL AND J. E. GREEDAN

Department of Chemistry and Institute for Materials Research, McMaster University, Hamilton, Ontario L8S 4M1 Canada

Received December 21, 1981; in revised form March 5, 1982

Solid solutions were prepared encompassing the entire composition range between $LaTiO_3$ and $GdTiO_3$. An anomaly in the magnetization–temperature data associated with magnetic ordering within the Ti^{3+} sublattice was observed for the phases $La_{0.5}Gd_{0.5}TiO_3$–$LaTiO_3$. $La_{0.3}Gd_{0.7}TiO_3$–$GdTiO_3$ appear to be two sublattice ferrimagnets. Anomalies in the magnetization–temperature curves observed for the compositions $La_{0.6}Gd_{0.4}TiO_3$–$La_{0.8}Gd_{0.2}TiO_3$ are consistent with spin glass behavior. The saturation magnetization of $GdTiO_3$ at 4.2K was measured to be 5.8 ± 0.2 μ_B/formula unit. Susceptibility data analyzed using the mean field model show a dramatic decrease in the strength of the ferromagnetic Ti^{3+}–Ti^{3+} exchange on the dilution of the Gd^{3+} sublattice by even 5% La^{3+}.

Introduction

In the preceding paper (*1*), the isostructural series of solid solutions $La_xY_{1-x}TiO_3$ was discussed. There is evidence for a change in sign of the Ti^{3+}–Ti^{3+} magnetic coupling between $LaTiO_3$ (antiferromagnetic) and $YTiO_3$ (ferromagnetic). Since both rare earths are diamagnetic, all magnetic effects observed can be attributed to the Ti^{3+} sublattice. The previous study indicates that the intermediate compositions have a complex magnetic structure.

The $La_xGd_{1-x}TiO_3$ series introduces the complication of a magnetic rare earth sublattice (Gd^{3+}–$4f^7$) but thereby creates the opportunity of studying the rare earth–transition metal interactions. Gd^{3+} was chosen since it is an *S* state ion, therefore crystal field effects should be negligible. From previous reports $GdTiO_3$ appears to be a 2 sublattice ferrimagnet, as are the other members of the series $RTiO_3$ (R = Tb–Yb) (*2*). Thus, as in the La–Y series, a change in sign of the Ti^{3+}–Ti^{3+} coupling is expected as the rare earth ratio is varied. Solid solutions of the form $La_xGd_{1-x}TiO_3$ (x = 0, 0.1, 0.3, 0.4, 0.5, 0.6, 0.7, 0.8, 0.9, 0.95, 0.98, 1.0) were prepared to monitor the change in magnetic properties across this series. A preliminary communication on this work has been published previously (*3*).

Sample Preparation and Analysis

All compounds were prepared by the reaction of appropriate mixtures of the rare earth oxides R_2O_3 (99.99%, from Research Chemicals) and Ti_2O_3. The rare earth oxides were prefired for 12 hr at 1000°C. Ti_2O_3 was prepared by arc-melting Ti sponge (99.99%, from Alpha Inorganics) and TiO_2 (99.95%, from Atomergic Chemicals) under argon.

The starting materials for the polycrystalline phases $GdTiO_3$–$La_{0.5}Gd_{0.5}TiO_3$ were sealed under argon in molybdenum crucibles and subjected to radio-frequency heat-

0022-4596/82/080204-09$02.00/0

ing near 1500°C for about 18 hr. The remaining La-rich phases were prepared by arc-melting. The reaction was carried out under argon on a rotating water-cooled copper hearth. The sample was molten for less than 3 min. Single-crystal samples of composition $La_{0.0}$–$La_{0.1}$ were also prepared. The starting materials were outgassed in a tri-arc crystal-growing furnace and the crystals were pulled from the melt at a rate of 1–2 cm/hr using the Czochralski technique (*4*). Crystals of about 20 mg (1- to 3-mm dimensions) consisting of one or two grains were extracted. Laue photographs indicated the misalignment of the grains to be at most 2°.

All products were analyzed by powder X-ray diffraction and thermal gravimetric analysis (TGA), measuring the weight gain upon air oxidation ($2RTi^{3+}O_3 + \frac{1}{2}O_2 \rightarrow R_2Ti_2^{4+}O_7$).

Cell constants were derived by a least-squares fit of 10–18 powder diffraction peaks which were corrected with an internal standard (Table I). All reflections could be indexed on the expected orthorhombic cell (*Pbnm*) consistent with the structure determination of the two end members of the series, $LaTiO_3$ and $GdTiO_3$ (*5*). A plot of (rare earth radius)^3 vs cell volume yields a smooth curve (Fig. 1).

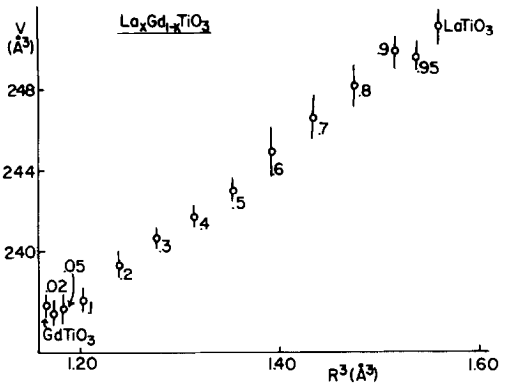

FIG. 1. Cell volume vs (rare earth radius)^3. Error bars represent one standard deviation.

TGA results (Table II) show close agreement with the desired stoichiometry, although slightly oxidized products are prevalent. The compounds prepared by the solid-state reaction were most prone to oxidation. The degree of oxidation seemed to increase roughly with firing temperature

TABLE I

LATTICE CONSTANTS FOR $La_xGd_{1-x}TiO_3$

	a (Å)	*b* (Å)	*c* (Å)	Volume (Å³)
$GdTiO_3$	5.409(5)	5.712(4)	7.681(7)	237.3(6)
$La_{0.02}$	5.409(5)	5.700(5)	7.683(6)	236.9(6)
$La_{0.05}$	5.414(5)	5.693(5)	7.694(8)	237.1(7)
$La_{0.1}$	5.429(5)	5.681(6)	7.705(8)	237.6(7)
$La_{0.2}$	5.450(5)	5.677(5)	7.733(9)	239.3(7)
$La_{0.3}$	5.475(6)	5.664(4)	7.762(5)	240.7(6)
$La_{0.4}$	5.497(6)	5.656(4)	7.789(6)	242.2(6)
$La_{0.5}$	5.516(6)	5.634(4)	7.820(6)	243.0(6)
$La_{0.6}$	5.532(11)	5.654(11)	7.830(12)	244.9(13)
$La_{0.7}$	5.561(9)	5.640(6)	7.864(16)	246.6(12)
$La_{0.8}$	5.593(10)	5.627(6)	7.885(11)	248.1(11)
$La_{0.9}$	5.622(4)	5.619(6)	7.908(11)	249.8(8)
$La_{0.95}$	5.621(4)	5.609(5)	7.917(12)	249.6(8)
$LaTiO_3$	5.633(11)	5.614(5)	7.940(6)	251.1(9)

TABLE II

OXIDATION WEIGHT GAIN (wtg) FOR $La_xGd_{1-x}TiO_3$

	wtg_{theo} (%)	wtg_{obs} (%)	$\left(\frac{wtg_{theo} - wtg_{obs}}{wtg_{theo}}\right) \times 100$ (%)
$LaTiO_3$	3.41	3.28	3.8
$La_{0.95}$	3.39	3.26	3.8
$La_{0.9}$	3.38	3.30	2.4
$La_{0.8}$	3.35	3.36	−.3
$La_{0.7}$	3.33	3.32	.3
$La_{0.6}$	3.30	3.27	1.0
$La_{0.5}$	3.28	3.31	−.8
$La_{0.4}$	3.25	3.21	1.2
$La_{0.3}$	3.23	3.29	−1.9
$La_{0.2}$[a]	3.21	3.07	4.4
$La_{0.1}$	3.18	3.13	1.6
$La_{0.05}$	3.17	3.23	−1.9
$La_{0.02}$	3.16	3.09	2.2
$GdTiO_3$	3.16	3.09	2.2

[a] $La_{0.2}Gd_{0.8}TiO_3$ was considered too oxidized for further study.

and duration. Single-phase products with the same nominal Gd/Ti ratio as those in Table II were obtained, and analyzed to as much as 37% oxidized. Critical temperatures of these oxidized samples were depressed by as much as 6K. The lattice constants of the oxidized samples were significantly smaller than those reported here, indicating the presence of Ti^{4+}. It is likely that the Ti^{4+} is associated with a charge compensation due to a rare earth cation deficiency. This is consistent with the nonstoichiometry reported in certain oxidized rare earth transition metal perovskites (*6*, *7*). In some preparations, slightly reduced titanium sesquioxide, $\sim Ti_2O_{2.99}$, was used to offset the tendency toward oxidation.

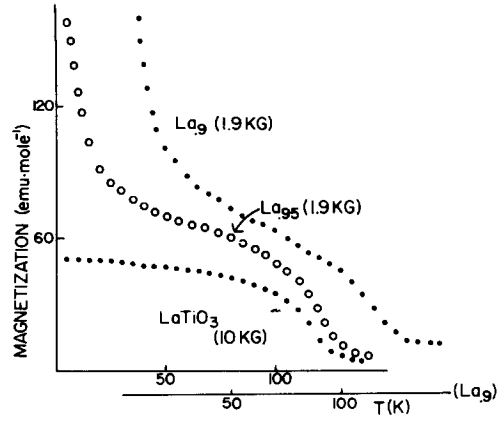

FIG. 2. Magnetization vs temperature for the phases $LaTiO_3$, $La_{0.95}Gd_{0.05}TiO_3$, and $La_{0.9}Gd_{0.1}TiO_3$. The applied field is given in brackets.

Magnetic Measurements

Magnetic data were obtained using a PAR vibrating sample magnetometer, calibrated by means of a high-purity nickel standard. Polycrystalline samples were pressed into 200- to 500-mg pellets. Ordering temperatures were derived from magnetization–temperature data collected at an applied field of 0.0045–1.0 T. For certain of the La-rich phases, M vs H data were collected at a number of temperatures and changes in the M vs T curves were studied as a function of applied field.

Susceptibility data were obtained for powder samples of composition $La_{0.0}$–$La_{0.5}$ in the range 4.2–200K at an applied field of ~1 T. The temperature was monitored using a gold–0.07% iron vs chromel thermocouple.

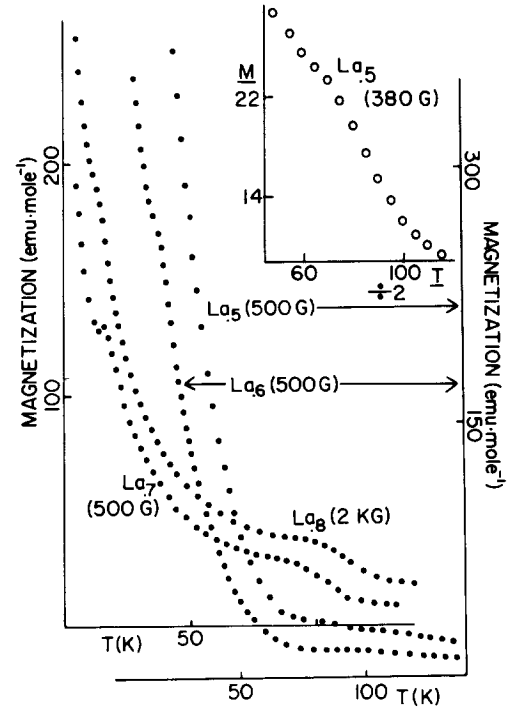

FIG. 3. Magnetization vs temperature for the phases $La_xGd_{1-x}TiO_3$ (x = 0.5, 0.6, 0.7, 0.8). The scale of the 70% La and 80% La compounds is on the left, that of the 50% La and 60% La compounds is on the right. The magnitude of M for the 50% La phase is one-half that shown. The units of M and T on the insert are the same as those in the main graph. The applied field is given in brackets.

Results and Discussion

As the La/Gd ratio is varied, changes in the low-field magnetization–temperature behavior occur over two separate intervals: one at low temperature below 20K, the other between 80–130K. In the composi-

tion range $La_{0.5}Gd_{0.5}TiO_3$–$La_{0.98}Gd_{0.02}TiO_3$ effects are present in both temperature regions simultaneously.

A critical temperature T_c is observed between 80–130K for the phases $La_{0.5}Gd_{0.5}TiO_3$–$LaTiO_3$ (Figs. 2, 3). As the Gd concentration increases, T_c drops and the anomaly itself becomes less pronounced. Since similar behavior is observed in the corresponding $La_xY_{1-x}TiO_3$ series (*1*), it is likely that this T_c is due to magnetic ordering within the Ti^{3+} sublattice. The shape of the M vs T curve for the phases $La_{0.5}Gd_{0.5}TiO_3$–$La_{0.8}Gd_{0.2}TiO_3$ is field dependent in this temperature range (Fig. 4). The anomalies observed are greatly suppressed on application of a large external field. As in $LaTiO_3$, hysteresis in isothermal magnetization–field curves was observed in $La_{0.7}Gd_{0.3}TiO_3$ below this T_c, but not above it. T_c for the phases $La_{0.9}Gd_{0.1}TiO_3$–$LaTiO_3$ were determined by linear extrapolation of M^2 vs T. T_c for the compositions $La_{0.5}Gd_{0.50}TiO_3$–$La_{0.8}Gd_{0.2}TiO_3$ were estimated as the point of inflection of the high-temperature anomaly (Table III).

The evolution of the magnetization curve in the low-temperature region below 20K is more complex and more easily described from the Gd-rich end of the series. The phases $GdTiO_3$–$La_{0.5}Gd_{15}TiO_3$ exhibit a smooth, well-defined drop in the magnetization in the region 12–33K. The slope becomes more shallow as the La concentration increases (Fig. 5). This is the only feature present in the magnetization–temperature data of the compounds $GdTiO_3$–$La_{0.4}Gd_{0.6}TiO_3$. $La_{0.5}Gd_{0.5}TiO_3$, however, exhibits two anomalies in its low-field magnetization vs temperature curve. A high-temperature T_c associated with magnetic ordering within the Ti^{3+} sublattice occurs near 85K (Fig. 3, insert). At 16K the magnetization drops sharply and smoothly with increasing temperature, exactly paralleling the behavior of the 30% La and 40% La compounds shown in Fig. 5. It is unclear whether or not this low-temperature anomaly at 16K represents a true critical temperature due to another distinct magnetic transition. Critical temperatures for these phases were estimated by linear extrapolation of M^2 vs T, although the unambigu-

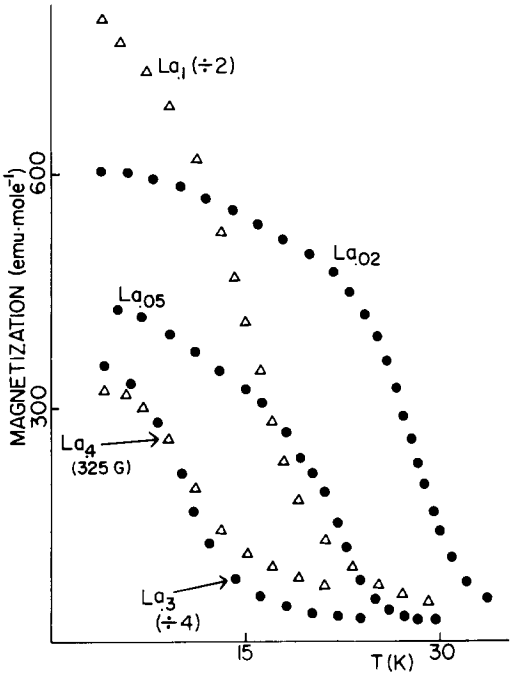

FIG. 5. Magnetization vs temperature for the phases $La_xGd_{1-x}TiO_3$ (x = 0.02, 0.05, 0.1, 0.3, 0.4). The magnitude of M for the 10% La phase is one-half that shown while the magnitude of M for the 30% La phase is one-quarter that shown. All data were obtained at an applied field of 45 G except that of the 40% La phase.

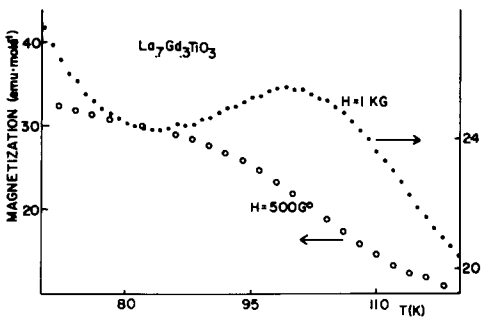

FIG. 4. Magnetization vs temperature for $La_{0.7}Gd_{0.3}TiO_3$ at applied fields of 500 and 1000 G.

TABLE III

CRITICAL TEMPERATURES (T_c), LOW-TEMPERATURE ANOMALIES (LTA), NEEL HYPERBOLA PARAMETERS (θ, C, ξ, θ'), AND MAGNETIC COUPLING CONSTANTS[a] (γ_{Gd-Ti}, γ_{Ti-Ti}, γ_{Gd-Gd}, FOR $La_xGd_{1-x}TiO_3$

	T_c (K)	LTA (K)	μSAT Ti^{3+} (B.M./ion)	θ	C	ξ	θ'	γTi–Gd (mole cm^{-3})	γTi–Ti (mole cm^{-3})	γGd–Gd (mole cm^{-3})	$C(Ti^{3+})$ (cm^3 K $mole^{-1}$)
$GdTiO_3$	33(2)		1.1 ± 0.2	−13(5)	7.9(1)	140(40)	30(5)	−23.8	40.6	0.3	0.01
$La_{0.02}$	30(2)		1.0 ± 0.2	−4(4)	7.77(9)	80(40)	30(10)	−17.6	43.4	1.0	0.06
$La_{0.05}$	22(2)		1.0 ± 0.2	−6(5)	7.4(1)	90(40)	15(8)	−18.1	7.2	0.9	−0.07
$La_{0.1}$	18(2)		1.0 ± 0.2	−3(3)	7.07(9)	60(30)	14(10)	−14.9	10.6	1.2	0.01
$La_{0.3}$	12(2)			−3(1)	5.60(4)	20(10)	8(7)	−9.1	5.3	0.6	0.10
$La_{0.4}$	14(2)			3.7(2)	5.0(1)						
$La_{0.5}$	85(7)	16(2)		−5.2(2)	4.01(1)						
$La_{0.6}$	93(5)	16(2)									
$La_{0.7}$	100(4)	14(2)									
$La_{0.8}$	114(3)	13(2)									
$La_{0.9}$	124(2)										
$La_{0.95}$	127(2)										
$LaTiO_3$	130(2)										

[a] In calculating these parameters, the value of $C(Ti^{3+})$ was taken to be 0.355 as reported for $YTiO_3$ in Ref. (*17*).

ously linear portion of the curve becomes less well defined as the La content grows. T_c decreases sharply to 12K for $La_{0.3}Gd_{0.7}TiO_3$, at which point it increases slightly for the 40% and 50% phases. A surprisingly similar quantitative correlation between T_c and La composition was observed in the Y-rich end of the $La_xY_{1-x}TiO_3$ series (*1*).

For the phases $La_{0.6}Gd_{0.4}TiO_3$–$La_{0.8}Gd_{0.2}TiO_3$, the smooth drop in the low-temperature magnetization observed for the Gd-rich compounds develops a fine structure. At low applied fields (500 G), an anomalous linear region appears in the neighborhood of 15K. The shape of this anomaly is strongly field dependent. Figure 6 shows, in the case of $La_{0.7}Gd_{0.3}TiO_3$, how this anomaly appears as a cusp at low applied field and becomes systematically suppressed as the field is increased. This behavior may suggest the evolution of a spin glass or mictomagnetic regime at these compositions. Although an actual cusp in the magnetization–temperature curve was observed only for the 70% La phase, a deviation from the Brillouin-like curvature of the magnetization–temperature curve near 15K persists for both the 60% La and 80% La compositions. It may be possible that the applied field of 500 G was large enough to suppress the cusp in these latter phases. Typically, applied fields in the neighborhood of 10 G are employed in spin glass studies (*8, 9*). Such small applied fields would result in magnetic moments too small to be measured reliably on our equipment.

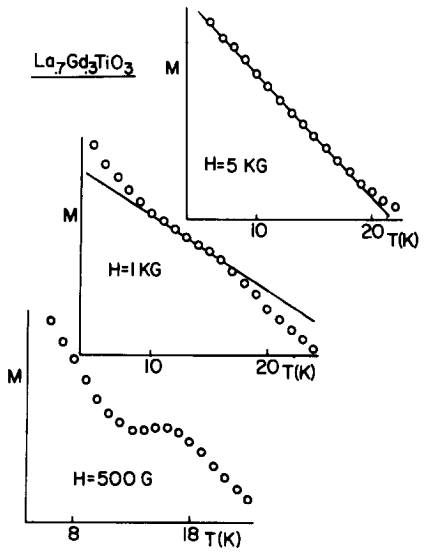

FIG. 6. Magnetization vs temperature for $La_{0.7}Gd_{0.3}TiO_3$ at applied fields of 500, 1000, and 5000 G.

While there is some uncertainty in the terminology used in describing these clustering effects (*10*) "spin glass" behavior has been observed in both metals (*11*) and insulators (*12*) over a wide concentration range of the clustering species. It has been proposed that one criterion for spin glass behavior may be the coexistence of competing positive and negative exchange interactions (*8, 12*). It is not unreasonable to expect both types of exchange in these phases, recalling the ferrimagnetic structure of the parent compound $GdTiO_3$.

For the most dilute Gd phases ($La_{0.98}Gd_{0.02}TiO_3$, $La_{0.95}Gd_{0.95}TiO_3$, and $La_{0.9}Gd_{0.1}TiO_3$) the fine structure disappears, resulting in a smooth decrease in the low-temperature magnetization as a function of increasing T. This feature is entirely absent in the corresponding La–Y phases. Figure 7 compares magnetization–temperature data for both $La_{0.1}$ phases collected at the same applied field. Assuming the Ti^{3+}–Ti^{3+} coupling to be the same in both compounds, we attempt to extract the effect of the rare earth interactions by a point by point subtraction of the two curves. Expressed as an inverse susceptibility (Fig. 8), this difference follows the Curie–Weiss law at low temperatures, yielding a negative value of θ and a Curie constant very close to the 0.787 predicted for a paramagnetic rare earth sublattice of $90\%La^{3+}/10\%Gd^{3+}$. These data point to the existence of short-range negative exchange interactions although the χ^{-1} vs T curve shows no evi-

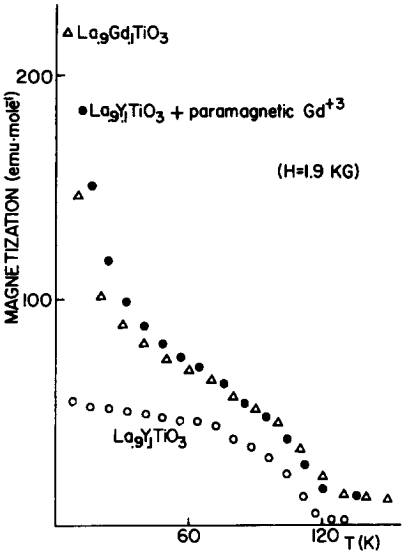

FIG. 7. Magnetization vs temperature for $La_{0.9}Gd_{0.1}TiO_3$ and $La_{0.9}Y_{0.1}TiO_3$ at an applied field of 1.9 kG. Also shown is the magnetization expected for a paramagnetic lattice of 90%La^{3+}/10%Gd^{3+} added to that obtained for $La_{0.9}Y_{0.1}TiO_3$.

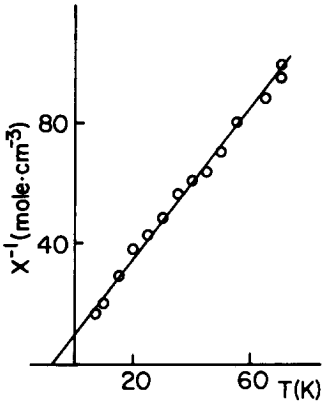

FIG. 8. Inverse susceptibility vs temperature derived by a subtraction of $M(La_{0.9}Gd_{0.1}TiO_3)$–$M(La_{0.9}Y_{0.1}TiO_3)$ in Fig. 7. The resulting values of θ and C are −8(1) and 0.80(2), respectively.

dence for a T_c above 4.2K. Note also (Fig. 7) that the sum of the magnetic moment calculated for a paramagnetic Gd^{3+} sublattice plus the signal measured for $La_{0.1}Y_{0.9}TiO_3$ yields a magnetization significantly larger than that observed for the corresponding La–Gd phase. This result further indicates predominant antiferromagnetic interactions in this temperature region. Recall that the low-temperature anomalies for the compositions $La_{0.6}Gd_{0.4}TiO_3$–$La_{0.8}Gd_{0.2}TiO_3$ occur around 15K, whereas the values of T_c for rare earth–rare earth coupling in the isostructural $RAlO_3$ compounds are usually much lower than this (*13*). The dilution of the Gd^{3+} sublattice by diamagnetic La^{3+} at these compositions ($La_{0.4}Gd_{0.6}$–$La_{0.8}Gd_{0.2}$) further discounts significant Gd^{3+}–Gd^{3+} interactions. It is probable that the behavior of the magnetization–temperature curves below 20K in the La-rich phases is governed by negative exchange interactions between the Gd^{3+} and Ti^{3+} ions. Antiparallel alignment of the ferromagnetically ordered R^{3+} and Ti^{3+} sublattices has been reported in the $RTiO_3$ series (*2*).

Magnetic saturation at 4.2K was achieved on crystalline samples of $GdTiO_3$ and $La_{0.02}Gd_{0.98}TiO_3$. Data for both the 5% and 10% La crystals were considered sufficiently close to permit extrapolation to infinite field (Fig. 9). At this end of the series, the tendency to saturation decreases with increasing La composition. Assuming a

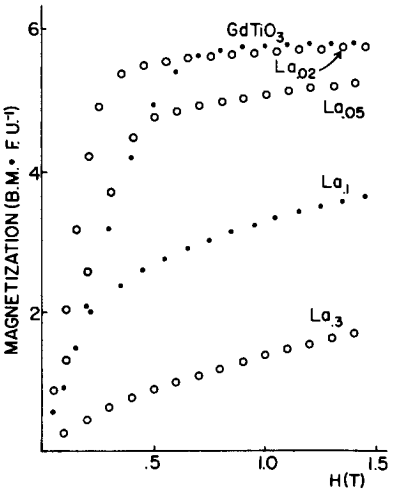

FIG. 9. Magnetization vs field for the phases $La_xGd_{1-x}TiO_3$ (x = 0, 0.02, 0.05, 0.1, 0.3). The data were obtained at 4.2K.

simple colinear ferrimagnetic structure, a saturation moment for Ti^{3+} of 1.1 ± 0.2 μ_B was estimated for $GdTiO_3$ and 1.0 ± 0.2 μ_B for the remaining three compounds. The $GdTiO_3$ saturation moment of 5.8 ± 0.2 μ_B/F.U. at 4.2K is in good agreement with the 6 μ_B/F.U. predicted by the simple two-sublattice model. The magnitude of the Ti^{3+} moment is consistent with a spin-only d^1 system, and not far from the value of 0.84 ± 0.01 μ_B found for ferromagnetic $YTiO_3$ (*14*).

The inverse susceptibility curves of the phases $GdTiO_3$–$La_{0.03}Gd_{0.7}TiO_3$ exhibit the hyperbolic shape characteristic of a two-sublattice ferrimagnet. Those of the 40% and 50% La compounds follow the Curie–Weiss law down to T_c (Fig. 10). These data were collected at an applied field of 1 T. At this field strength, the anomaly in the low-field M vs T curve of $La_{0.5}Gd_{0.5}TiO_3$ disappears. Assuming antiparallel alignment of the ferromagnetically ordered Gd^{3+} and Ti^{3+} sublattices, this theory predicts χ^{-1} vs T to fit a four-parameter hyperbola of the form

$$\chi^{-1} = \frac{T - \theta}{C} - \frac{\xi}{T - \theta'} \qquad (1)$$

where C^{-1} is the limiting slope of the curve in the paramagnetic region and θ is its intercept. ξ and θ' are determined by the curvature in the lower temperature region near T_c. From these four parameters, coupling constants, γ, can be calculated indicating the sign and relative magnitudes of the exchange interactions in the system (*15, 16*) (Table III). As $GdTiO_3$ is doped with La, the antiferromagnetic exchange between the Ti^{3+} and Gd^{3+} weakens as expected with dilution of the magnetic rare earth sublattice. The ferromagnetic Ti^{3+}–Ti^{3+} coupling drops even more steeply with increasing La concentration. This is consistent with the predominance of antiferromagnetic exchange in the La-rich end of the series. The Gd^{3+}–Gd^{3+} interaction is small and positive and does not vary systematically.

Assuming a colinear ferrimagnetic model, the Curie constant for Ti^{3+} in these compounds can be derived from the slope of χ^{-1} in the paramagnetic region (Table III). In all cases, $C(Ti^{3+})$ is substantially reduced from the free ion value of 0.37. Unfortunately, these values are small with respect to the estimated experimental error of 3%.

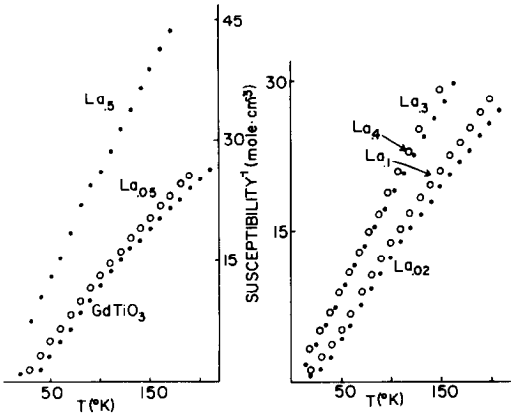

FIG. 10. Inverse susceptibility vs temperature for the phases $La_xGd_{1-x}TiO_3$ (x = 0, 0.02, 0.05, 0.1, 0.3, 0.4, 0.5). The data were collected at an applied field of about 1 T.

Conclusions

The magnetic behavior of the solid solutions $La_xGd_{1-x}TiO_3$ may be summarized by means of a magnetic phase diagram (Fig. 11).

(*I*) $LaTiO_3$–$La_{0.9}Gd_{0.1}TiO_3$

The M vs T curves of these compounds display a high-temperture anomaly most likely corresponding to a canted antiferromagnetic ordering of the Ti^{3+} sublattice. The low-temperature magnetization data imply antiferromagnetic exchange interactions between the Gd^{3+} and Ti^{3+} ions, although there is no evidence for magnetic ordering of the Gd^{3+} ions above 4.2K.

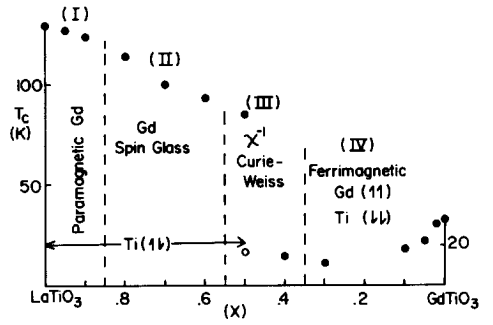

FIG. 11. Magnetic phase diagram for the system $La_xGd_{1-x}TiO_3$. The critical temperature (T_c) is plotted on the vertical scale and the compositional parameter (χ) is plotted on the horizontal scale.

(*II*) $La_{0.8}Gd_{0.2}TiO_3$–$La_{0.6}Gd_{0.4}TiO_3$

These compounds also exhibit a high-temperature anomaly associated with ordering within the Ti^{3+} sublattice. The shape of the magnetization–temperature curve below 20K is field dependent, perhaps indicative of spin glass behavior.

(*III*) $La_{0.5}Gd_{0.5}TiO_3$–$La_{0.4}Gd_{0.6}TiO_3$

The Ti^{3+}–Ti^{3+} exchange most likely changes sign in this composition range. χ^{-1} data collected at 1 T for both compounds follow the Curie–Weiss law down to the low-temperature anomaly.

(*IV*) $La_{0.3}Gd_{0.7}TiO_3$–$GdTiO_3$

The inverse susceptibility data for these phases can be fitted to a two-sublattice ferrimagnetic model. Analysis of the susceptibility data on the molecular field model yielded a Ti^{3+}–Ti^{3+} coupling constant which showed a precipitous drop between $La_{0.02}Gd_{0.98}TiO_3$ and $La_{0.05}Gd_{0.95}TiO_3$. Assuming the two-sublattice ferrimagnetic model, magnetic saturation measurements at 4.2K yielded a full 1 μ_B Ti^{3+} moment for the compositions $La_{0.1}Gd_{0.9}TiO_3$–$GdTiO_3$.

Acknowledgments

We wish to thank Dr. C. V. Stager for the use of his magnetometer and Mr. Gord Hewitson for his assistance in collecting these data. The financial support of the National Science and Engineering Research Council of Canada is acknowledged.

References

1. J. P. GORAL, J. E. GREEDAN, AND D. A. MACLEAN, *J. Solid State Chem.*, in press.
2. C. W. TURNER AND J. E. GREEDAN, *J. Solid State Chem.* **34,** 207 (1980).
3. J. P. GORAL AND J. E. GREEDAN, *in* "The Rare Earths in Modern Science and Technology," Vol. III, (G. J. McCarthy, J. J. Rhyne, and H. B. Silber, Eds.), Plenum Press, New York, (1982).
4. R. A. LAUDISE, "The Growth of Single Crystals," Prentice–Hall, Englewood, New Jersey (1970).
5. D. A. MACLEAN, HOK-NAM NG, AND J. E. GREEDAN, *J. Solid State Chem.* **30,** 35 (1979).
6. D. A. MACLEAN AND J. E. GREEDAN, *Inorg. Chem.* **20,** 1025 (1981).
7. B. C. TOFIELD AND W. R. SCOTT, *J. Solid State Chem.* **10,** 183 (1974).
8. P. A. BECK, *Phys. Rev. B* **23,** 2290 (1981).
9. J. L. THOLENCE, F. HOLTZBERG, T. R. MCGUIRE, AND S. VON MOLNAR, *J. Appl. Phys.* **50,** 7350 (1979).
10. J. A. MYDOSH, *J. Magn. Mag. Mater.* **7,** 237 (1978).
11. A. K. MUKHOPADHYAY, R. D. SCHULL, AND P. A. BECK, *J. Less-Common Met.* **43,** 69 (1975).
12. H. MALETTA AND W. FELSCH, *Phys. Rev. B* **20,** 1245 (1979).
13. J. B. GOODENOUGH AND J. M. LONGO, "Crystallographic and Magnetic Properties of Perovskites and Perovskite-Related Compounds," Landolt-Bornstein Tabellen, New Series III/4a, Springer-Verlag, Berlin (1970); see, for instance, B. K. BLAZEY AND H. ROHRER, *Helv. Phys. Acta* **40,** 370 (1967).
14. J. D. GARRETT, J. E. GREEDAN, AND D. A. MACLEAN, *Mater. Res. Bull.* **16,** 145 (1981).
15. J. S. SMART, "Effective Field Theories of Magnetism," Chap. 12, Saunders, Philadelphia (1966).
16. A. H. MORRISH, "The Physical Principles of Magnetism," Chap. 9, Wiley, New York (1965).
17. D. JOHNSTON, Ph.D. thesis, University of California, San Diego, 1975.